


Misalignment-robust zigzag gate geometry for valley filtering with helical point contacts

Antonio L. R. Manesco^{1, †} 

¹ Kavli Institute of Nanoscience, Delft University of Technology, Delft 2600 GA, The Netherlands

[†]am@antoniomanesco.org

August 13, 2024

Abstract

Many experimental works reported the generation of valley-polarized currents in two-dimensional materials. However, most efforts require the application of external magnetic fields. Gate-defined valley-helical narrow channels offer a magnetic field-free approach to generate valley currents. However, achieving perfect helical transport in such gate-defined devices remains challenging due to stringent requirements for gate alignment. Misalignments lead to the presence of non-helical states that suppress the efficiency of these devices. Here, we propose an alternative gate layout to overcome the fabrication challenges. Our layout creates a series of helical quantum point contacts that suppress the transmission of non-helical modes. We show that such a layout can be implemented with four layers of independent gates or two layers of split gates. Thus, our approach offers a robust magnetic field-free platform to generate valley-polarized currents.

1 Introduction

Recent experiments have consistently observed valley phenomena in graphene, such as valley order in graphene multilayers [1–6], valley-polarized states in gate-defined quantum dots [7, 8], and valley jetting through quantum point contacts [9, 10]. These observations are a direct consequence of high-mobility graphene samples obtained with hexagonal boron nitride encapsulation [11, 12], graphite back gates [13–15], and gate-controllable bandgaps [16–22]. This progress motivated a search for novel valleytronics devices, such as the generation and detection of valley currents in Bernal-stacked bilayer graphene either via valley-to-charge conversion [7, 8] or electron collimation [10].

These recent experiments, however, rely on controlling valleys with magnetic fields. Gate-defined valley-helical narrow channels offer a magnetic-field-free alternative for generation and detection of valley-polarized currents [23–31]. A set of in-gap modes exist at an interface where the displacement field changes sign, for example with two sets of double-gates as the layout depicted in Fig. 1 (a). Because the valley propagation is unidirectional, as shown in Fig. 1 (c), the electrical current injected through these channels is filtered depending on their valley composition.¹

However, experimental works and realistic simulations thus far have failed to achieve perfect filtering efficiency [25, 27–29]. The main reason for the observed suboptimal efficiency of gate-defined valley filters is the presence of additional non-helical modes [27, 29, 34]. In the absence of intervalley scattering, the two sources of additional channels are the screening

¹The details in the numerical calculations shown in these panels and throughout the manuscript are described in Appendix A. The code and data generated for this manuscript is fully available in Zenodo [32]. The numerical implementation was largely based on [33].

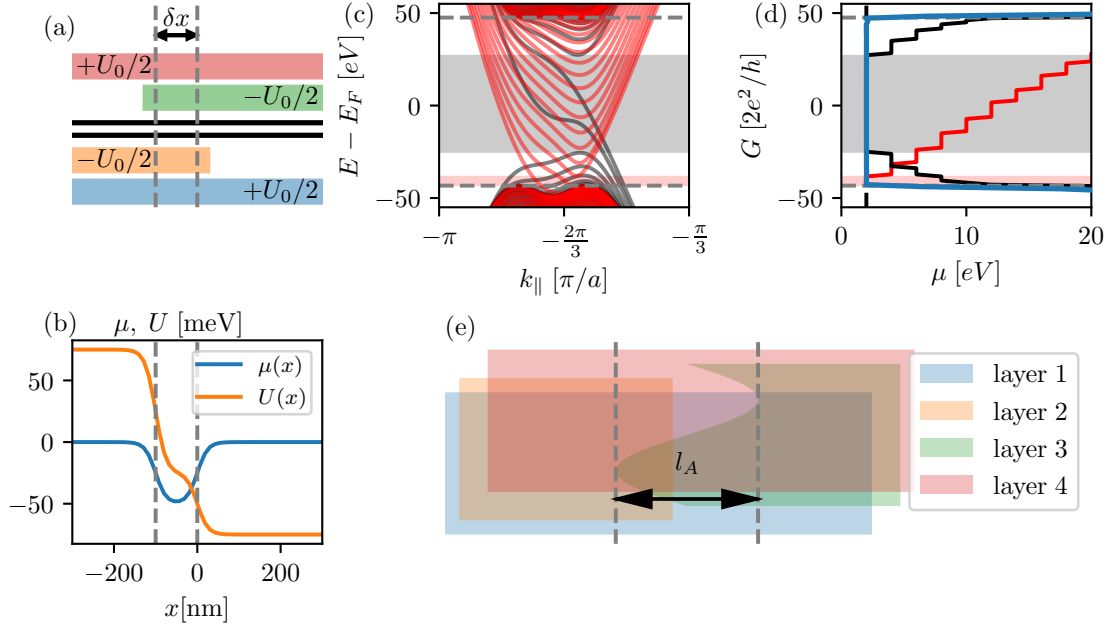


Figure 1: (a) Possible gate configuration to obtain valley-helical channels. Four layers of gates create two regions with opposite displacement fields, generating a layer imbalance shown in blue in panel (b). A misalignment δx between the two layers results in a modulation of the local chemical potential $\mu(x)$ shown in orange in panel (b). (c) Bandstructure of valley-helical ribbon with $U_0 = 100\text{meV}$ and a screening length $\chi = 25\text{nm}$ at valley K . The vertical dashed lines indicate the bulk gap. The black lines show the dispersion relation of a ribbon with $\delta x = 0$ and in red with $\delta x = 100\text{nm}$. In both cases, we observe non-helical states within the bulk gap. The black and red shaded areas indicate the window with only helical modes for $\delta x = 0$ and $\delta x = 100\text{nm}$. (d) Conductance across a ribbon with $\delta = 0$ (black), $\delta x = 100\text{nm}$ (red), and across a device with a zigzag-like gate layout shown in panel (e) (blue). The layout shown in panel (e) suppresses the transmission of extra modes, resulting in quantized conductance at $4e^2/h$ (dashed horizontal black line in panel (d)).

of the gate potential and misalignment between top and bottom gates, as illustrated in Fig. 1 (b, c). Because those channels are non-helical, the valley propagation is no longer unidirectional. Only recently, quantized conductance along these helical channels was observed in the absence of a magnetic field by using another gate layer [30].

In this work, we propose the zigzag-like gate layout shown in Fig. 1 (e) that filters the transmission of non-helical modes for any type of gate misalignment smaller than the oscillation amplitude. The geometry works with both four gate layers or two layers of split gates, making it compatible with recent advancements in the lithography of graphite gates [15]. Our proposal does not require gate alignment, narrow channels, or additional gate layers. The numerical simulations of this device show that the filtering efficiency is limited only by intervalley scattering and tunneling of the additional modes. While intervalley scattering is nearly suppressed under the smooth electrostatic potential landscapes caused by screening effects, tunneling is exponentially suppressed by the filter length. Therefore, our proposal effectively achieves nearly perfect valley-helical transport, as shown in Fig. 1 (d). Moreover, our findings also suggest a method to fabricate valley-helical quantum point contacts with fewer constraints on fabrication than narrow channels. This simplification

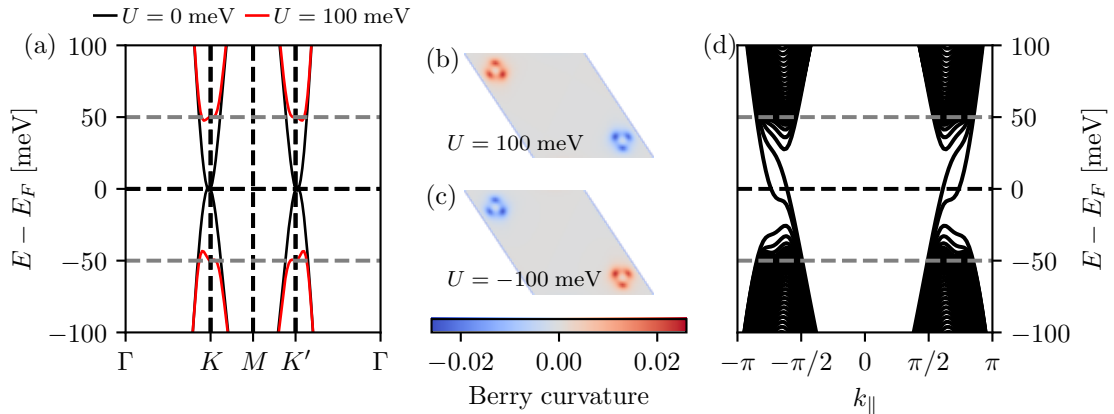


Figure 2: (a) Bulk bandstructure of Bernal bilayer graphene with $U_0 = 0$ and $U_0 = 100$ meV. A sublattice imbalance U_0 opens a gap in the band structure. Berry curvature for (b) $U_0 = 100$ meV and (c) $U_0 = -100$ meV. Due to time-reversal symmetry, the two valleys have opposite Berry curvature. However, the Berry curvature changes sign with layer imbalance. The valley Chern number changes across an interface where U flips sign results in the in-gap valley helical modes shown in panel (d).

facilitates the fabrication of more complex valleytronics devices, for example by integrating valley switches [30], valley probes [31], and Hall bars [15] in a single device.

2 Gate-defined valley-helical channels

2.1 Gate-controllable gap inversion

Due to a combination of mirror and time-reversal symmetries, the conduction and valence bands in graphene are degenerate at the corners of the Brillouin zone, as shown in Fig. 2 (a). This degeneracy makes graphene a gapless semiconductor. Thus, modulations of the carrier density are insufficient to confine electrons due to Klein tunneling [35, 36]. However, in graphene multilayers, the mirror symmetry is broken by the application of an out-of-plane electric field. The potential imbalance U between the layers opens a gap in the electronic structure [16–22] as depicted by Fig. 2 (a). Therefore, it is possible to control the band gap of graphene multilayers with double-gated devices [22, 37].

In Bernal bilayer graphene, the Berry curvature at each valley depends on the direction of the external electric field, shown in Fig. 2 (b, c). Thus, at the interface of two regions with opposite displacement fields, the valley Chern number changes. As a consequence, these interfaces host topological valley helical channels. In Fig. 2 (d) we show the dispersion of a nanoribbon with a switching layer imbalance. Due to the valley Chern number switch at this interface, in-gap valley-helical states propagate along the interface. The helicity of these channels thus constrains the electronic motion in a single direction. For this reason, these channels were proposed as valley filters.

2.2 In-gap non-topological modes

A perfect valley filter requires a gate geometry that prevents the transmission of non-topological states within the bulk gap. However, the finite distance between split gates,

screening of the electric fields, and misalignment of top and bottom gates change the carrier density in these electrically defined channels. As a result, additional non-topological modes also propagate within the bulk gap. We illustrate this by comparing the bulk gap in Fig. 2 (a) and the reduced topological gap due to electrostatic screening in Fig. 2 (d). We also show the dispersion of a channel with misalignment between top and bottom gates in Fig. 1 (c).

We observe the presence of non-helical states in transport as the conductance goes above $G = 4e^2/h$ as shown in Fig. 1 (d). Time-reversal symmetry preserves valley degeneracy, as shown in Fig. 2 (d), resulting in the conductance steps of $4e^2/h$ in Fig. 1 (d). Because both valleys transmit non-topological modes, pure helical transport is thus only possible within the energy windows shown in Fig. 1 (c, d). Therefore, these additional modes limit the operational window of valley filters. This is a limitation even in recent experiments that observed for the first time valley-helical transport without external magnetic fields.

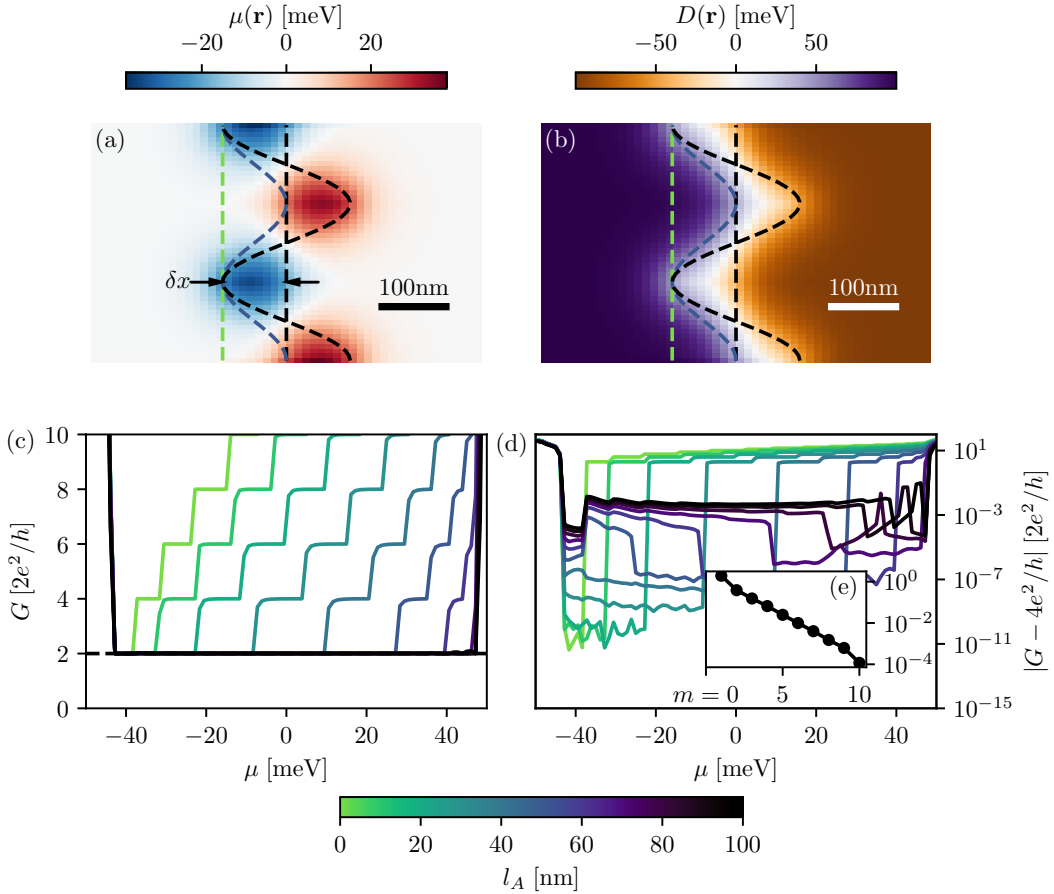


Figure 3: Local chemical potential (a) and layer imbalance (b) resulting from the gate layout illustrated in Fig. 1. The vertical dashed line shows the location of the potential step in the lower set of gates. The colored lines indicate the potential step in the upper set of gates as a function of the amplitude l_A of the periodic modulation. (c) Conductance as a function of the global chemical potential μ and l_A . We observe approximate quantized conductance at $4e^2/h$ as long as $\delta x \lesssim l_A/2$. (d) Deviations from quantized conductance showing a residual value $G \sim 10^{-3}e^2/h$. We attribute this residual value to tunneling between the puddles shown in panels (a) and (b). (e) Exponential suppression of the residual conductance as the number of crossings m between the potential edges increases.

3 Zigzag geometry

To overcome this limitation, we propose an alternative gate layout, for which one of the gate layers has a zigzag-like pattern shown in Fig. 1 (e). Once the zigzag pattern amplitude l_A is larger than the alignment precision, it creates bottlenecks preventing additional modes from propagating. The resulting local chemical potential and layer imbalance in graphene due to the overlaps between gates is shown in Fig. 3 (a,b). Although the resulting device still has no spectral gap due to the puddles with non-zero chemical potential visible in Fig. 3 (a), these puddles are connected by “valley-helical point contacts” shown in Fig. 3 (b). The pn -junction between those puddles also suppresses the propagation of non-helical modes between the two regions.

The helical point contacts bottleneck the transmission and the filter recovers nearly maximal efficiency, *i.e.* only the helical modes transmit and the conductance remains nearly constant at $4e^2/h$. We show in Fig. 3 (c) the conductance across a single helical point contact. We observe that the transmission of non-helical modes is suppressed when the upper and lower gate layers cross, which occurs when $\delta x \lesssim l_A/2$. The residual conductance $|G - 4e^2/h|$ shown in Fig. 3 (d) remains non-zero due to tunneling between the puddles. Therefore, this residual transmission is exponentially suppressed as a function of the number of periods m of the gate modulation as shown in Fig. 3 (e). Thus, the only constraints in

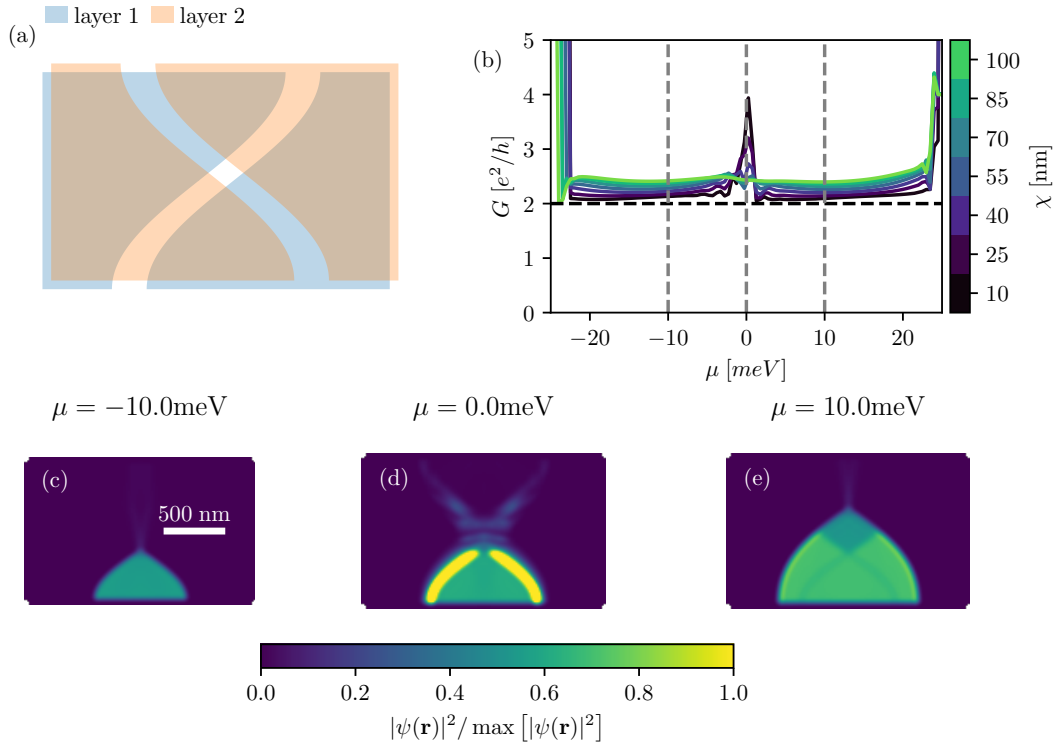


Figure 4: (a) Illustration of the gate layout with a single crossing point with split gates. (b) Conductance across a device with the layout geometry from panel (a) as a function of the global chemical potential μ and screening length χ . We observe that the residual conductance above $4e^2/h$ increases with χ due to higher tunneling probabilities. The conductance shows a peak at $\mu = 0$ due to additional transmission probabilities through the gap between split gates as we can observe by comparing the scattering wavefunctions in panel (d) with (c) and (e).

the gate layout are: (i) the amplitude l_A of the gate modulation period is larger than the expected misalignment during fabrication, and (ii) the periodically modulated region is sufficiently long to suppress tunneling events.

Due to possible complications in fabricating the layout in Fig. 1 (a, e) with four layers of gates, we also calculate the conductance of a device with similar zigzag geometry but two layers of split shown in Fig 4 (a). Despite the distance of 200nm between gates used in the simulations, the transmission of non-topological in-gap states is still suppressed, as shown in Fig 4 (b). Additionally to the conductance plateau at $G \approx 4e^2/h$, we also observe a conductance peak at charge neutrality. By inspecting the scattering wavefunctions, shown in Fig. 4 (c-e), we conclude that this resonance peak occurs due to additional propagating modes within the split-gates gap. Thus, we demonstrate that both the four-gate layout shown in Fig. 1 (e) and the double-split-gate geometry in Fig. 4 (a) can be used to fabricate valley-helical quantum point contacts without gate-defined narrow channels.

4 Conclusion

We proposed a gate layout that suppresses the transmission of non-topological states in gate-defined valley-helical channels. Our layout consists of a zigzag-like pattern in one of the gate layers that creates a series of valley-helical point contacts. As long as the amplitude of the zigzag modulations is sufficiently large, our design is resilient against any type of gate misalignment. The limiting factors in the efficiency of our layout are intervalley scattering and tunneling between charge puddles. We showed that the latter can be minimized by increasing the number of periods of the filter, while the former is expected to be small in ballistic gate-defined devices. Moreover, we show that our layout can be fabricated both with four layers of gates, or two layers of split gates. Our results also suggest a simple and yet experimentally unexplored layout to fabricate gate-defined valley-helical quantum point contacts.

Acknowledgements

We acknowledge Kostas Vilkelis, Isidora Araya-Day, and Anton Akhmerov for fruitful discussions. We also thank Valla Fatemi, Josep Ingla-Aynés, and Luca Banszerus for their input on the experimental implementation of our proposal. We thank Anton Akhmerov, Josep Ingla-Aynés, and Kushagra Aggarwal for the feedback on the manuscript.

Data availability

The code and data generated for this manuscript and additional datasets are fully available on Zenodo [32].

References

- [1] H. Zhou, L. Holleis, Y. Saito, L. Cohen, W. Huynh, C. L. Patterson, F. Yang, T. Taniguchi, K. Watanabe and A. F. Young, *Isospin magnetism and spin-polarized superconductivity in bernal bilayer graphene*, Science **375**(6582), 774–778 (2022), doi:[10.1126/science.abm8386](https://doi.org/10.1126/science.abm8386).

- [2] K. Huang, H. Fu, D. R. Hickey, N. Alem, X. Lin, K. Watanabe, T. Taniguchi and J. Zhu, *Valley isospin controlled fractional quantum hall states in bilayer graphene*, Physical Review X **12**(3) (2022), doi:[10.1103/physrevx.12.031019](https://doi.org/10.1103/physrevx.12.031019).
- [3] S. C. de la Barrera, S. Aronson, Z. Zheng, K. Watanabe, T. Taniguchi, Q. Ma, P. Jarillo-Herrero and R. Ashoori, *Cascade of isospin phase transitions in bernal-stacked bilayer graphene at zero magnetic field*, Nature Physics **18**(7), 771–775 (2022), doi:[10.1038/s41567-022-01616-w](https://doi.org/10.1038/s41567-022-01616-w).
- [4] Y. Cao, V. Fatemi, A. Demir, S. Fang, S. L. Tomarken, J. Y. Luo, J. D. Sanchez-Yamagishi, K. Watanabe, T. Taniguchi, E. Kaxiras, R. C. Ashoori and P. Jarillo-Herrero, *Correlated insulator behaviour at half-filling in magic-angle graphene superlattices*, Nature **556**(7699), 80–84 (2018), doi:[10.1038/nature26154](https://doi.org/10.1038/nature26154).
- [5] S. Chatterjee, T. Wang, E. Berg and M. P. Zaletel, *Inter-valley coherent order and isospin fluctuation mediated superconductivity in rhombohedral trilayer graphene*, Nature Communications **13**(1) (2022), doi:[10.1038/s41467-022-33561-w](https://doi.org/10.1038/s41467-022-33561-w).
- [6] K. P. Nuckolls, R. L. Lee, M. Oh, D. Wong, T. Soejima, J. P. Hong, D. Călugăru, J. Herzog-Arbeitman, B. A. Bernevig, K. Watanabe, T. Taniguchi, N. Regnault *et al.*, *Quantum textures of the many-body wavefunctions in magic-angle graphene*, Nature **620**(7974), 525–532 (2023), doi:[10.1038/s41586-023-06226-x](https://doi.org/10.1038/s41586-023-06226-x).
- [7] M. Eich, F. Herman, R. Pisoni, H. Overweg, A. Kurzman, Y. Lee, P. Rickhaus, K. Watanabe, T. Taniguchi, M. Sigrist, T. Ihn and K. Ensslin, *Spin and valley states in gate-defined bilayer graphene quantum dots*, Physical Review X **8**(3) (2018), doi:[10.1103/physrevx.8.031023](https://doi.org/10.1103/physrevx.8.031023).
- [8] L. Banszerus, B. Frohn, A. Epping, D. Neumaier, K. Watanabe, T. Taniguchi and C. Stampfer, *Gate-defined electron-hole double dots in bilayer graphene*, Nano Letters **18**(8), 4785–4790 (2018), doi:[10.1021/acs.nanolett.8b01303](https://doi.org/10.1021/acs.nanolett.8b01303).
- [9] C. Gold, A. Knothe, A. Kurzman, A. Garcia-Ruiz, K. Watanabe, T. Taniguchi, V. Fal’ko, K. Ensslin and T. Ihn, *Coherent jetting from a gate-defined channel in bilayer graphene*, Physical Review Letters **127**(4) (2021), doi:[10.1103/physrevlett.127.046801](https://doi.org/10.1103/physrevlett.127.046801).
- [10] J. Ingle-Aynés, A. L. R. Manesco, T. S. Ghiasi, K. Watanabe, T. Taniguchi and H. S. J. van der Zant, *A ballistic electron source with magnetically-controlled valley polarization in bilayer graphene*, doi:[10.48550/ARXIV.2310.15293](https://doi.org/10.48550/ARXIV.2310.15293) (2023).
- [11] C. R. Dean, A. F. Young, I. Meric, C. Lee, L. Wang, S. Sorgenfrei, K. Watanabe, T. Taniguchi, P. Kim, K. L. Shepard and J. Hone, *Boron nitride substrates for high-quality graphene electronics*, Nature Nanotechnology **5**(10), 722–726 (2010), doi:[10.1038/mnano.2010.172](https://doi.org/10.1038/mnano.2010.172).
- [12] C. Dean, A. Young, L. Wang, I. Meric, G.-H. Lee, K. Watanabe, T. Taniguchi, K. Shepard, P. Kim and J. Hone, *Graphene based heterostructures*, Solid State Communications **152**(15), 1275–1282 (2012), doi:[10.1016/j.ssc.2012.04.021](https://doi.org/10.1016/j.ssc.2012.04.021).
- [13] A. F. Young, J. D. Sanchez-Yamagishi, B. Hunt, S. H. Choi, K. Watanabe, T. Taniguchi, R. C. Ashoori and P. Jarillo-Herrero, *Tunable symmetry breaking and helical edge transport in a graphene quantum spin hall state*, Nature **505**(7484), 528–532 (2013), doi:[10.1038/nature12800](https://doi.org/10.1038/nature12800).

- [14] H. Overweg, H. Eggimann, X. Chen, S. Slizovskiy, M. Eich, R. Pisoni, Y. Lee, P. Rickhaus, K. Watanabe, T. Taniguchi, V. Fal'ko, T. Ihn *et al.*, *Electrostatically induced quantum point contacts in bilayer graphene*, Nano Letters **18**(1), 553–559 (2017), doi:[10.1021/acs.nanolett.7b04666](https://doi.org/10.1021/acs.nanolett.7b04666).
- [15] L. A. Cohen, N. L. Samuelson, T. Wang, K. Klocke, C. C. Reeves, T. Taniguchi, K. Watanabe, S. Vijay, M. P. Zaletel and A. F. Young, *Nanoscale electrostatic control in ultraclean van der waals heterostructures by local anodic oxidation of graphite gates*, Nature Physics **19**(10), 1502–1508 (2023), doi:[10.1038/s41567-023-02114-3](https://doi.org/10.1038/s41567-023-02114-3).
- [16] E. McCann, *Asymmetry gap in the electronic band structure of bilayer graphene*, Physical Review B **74**(16) (2006), doi:[10.1103/physrevb.74.161403](https://doi.org/10.1103/physrevb.74.161403).
- [17] E. V. Castro, K. S. Novoselov, S. V. Morozov, N. M. R. Peres, J. M. B. L. dos Santos, J. Nilsson, F. Guinea, A. K. Geim and A. H. C. Neto, *Biased bilayer graphene: Semiconductor with a gap tunable by the electric field effect*, Phys. Rev. Lett. **99**, 216802 (2007), doi:[10.1103/PhysRevLett.99.216802](https://doi.org/10.1103/PhysRevLett.99.216802).
- [18] H. Min, B. Sahu, S. K. Banerjee and A. H. MacDonald, *Ab initio theory of gate induced gaps in graphene bilayers*, Physical Review B **75**(15) (2007), doi:[10.1103/physrevb.75.155115](https://doi.org/10.1103/physrevb.75.155115).
- [19] J. B. Oostinga, H. B. Heersche, X. Liu, A. F. Morpurgo and L. M. K. Vandersypen, *Gate-induced insulating state in bilayer graphene devices*, Nature Materials **7**(2), 151–157 (2007), doi:[10.1038/nmat2082](https://doi.org/10.1038/nmat2082).
- [20] Y. Zhang, T.-T. Tang, C. Girit, Z. Hao, M. C. Martin, A. Zettl, M. F. Crommie, Y. R. Shen and F. Wang, *Direct observation of a widely tunable bandgap in bilayer graphene*, Nature **459**(7248), 820–823 (2009), doi:[10.1038/nature08105](https://doi.org/10.1038/nature08105).
- [21] A. B. Kuzmenko, I. Crassee, D. van der Marel, P. Blake and K. S. Novoselov, *Determination of the gate-tunable band gap and tight-binding parameters in bilayer graphene using infrared spectroscopy*, Phys. Rev. B **80**, 165406 (2009), doi:[10.1103/PhysRevB.80.165406](https://doi.org/10.1103/PhysRevB.80.165406).
- [22] K. F. Mak, C. H. Lui, J. Shan and T. F. Heinz, *Observation of an electric-field-induced band gap in bilayer graphene by infrared spectroscopy*, Physical Review Letters **102**(25) (2009), doi:[10.1103/physrevlett.102.256405](https://doi.org/10.1103/physrevlett.102.256405).
- [23] I. Martin, Y. M. Blanter and A. F. Morpurgo, *Topological confinement in bilayer graphene*, Physical Review Letters **100**(3) (2008), doi:[10.1103/physrevlett.100.036804](https://doi.org/10.1103/physrevlett.100.036804).
- [24] J. Jung, F. Zhang, Z. Qiao and A. H. MacDonald, *Valley-hall kink and edge states in multilayer graphene*, Physical Review B **84**(7) (2011), doi:[10.1103/physrevb.84.075418](https://doi.org/10.1103/physrevb.84.075418).
- [25] T. Fabian, *Simulation of Electronic Transport in Graphene Systems*, Ph.D. thesis, doi:[10.34726/HSS.2021.88068](https://doi.org/10.34726/HSS.2021.88068) (2021).
- [26] K. Prikoszovich, *Valley-filters using kink states in bilayer graphene* (2022), doi:[10.34726/HSS.2022.93461](https://doi.org/10.34726/HSS.2022.93461).
- [27] J. Li, K. Wang, K. J. McFaul, Z. Zern, Y. Ren, K. Watanabe, T. Taniguchi, Z. Qiao and J. Zhu, *Gate-controlled topological conducting channels in bilayer graphene*, Nature Nanotechnology **11**(12), 1060–1065 (2016), doi:[10.1038/nnano.2016.158](https://doi.org/10.1038/nnano.2016.158).

- [28] Y. Kang, X. Ni, X. Cheng, A. B. Khanikaev and A. Z. Genack, *Pseudo-spin–valley coupled edge states in a photonic topological insulator*, Nature Communications **9**(1) (2018), doi:[10.1038/s41467-018-05408-w](https://doi.org/10.1038/s41467-018-05408-w).
- [29] J. Li, R.-X. Zhang, Z. Yin, J. Zhang, K. Watanabe, T. Taniguchi, C. Liu and J. Zhu, *A valley valve and electron beam splitter*, Science **362**(6419), 1149–1152 (2018), doi:[10.1126/science.aao5989](https://doi.org/10.1126/science.aao5989).
- [30] K. Huang, H. Fu, K. Watanabe, T. Taniguchi and J. Zhu, *High-temperature quantum valley hall effect with quantized resistance and a topological switch*, Science (2024), doi:[10.1126/science.adj3742](https://doi.org/10.1126/science.adj3742).
- [31] J. D. T. Luna, K. Vilkelis and A. L. Manesco, *Probing valley phenomena with gate-defined valley splitters*, arXiv preprint arXiv:2405.00538 (2024).
- [32] A. L. Rigotti Manesco, *Valley filtering with gate-defined helical point contacts in graphene multilayers*, doi:[10.5281/zenodo.13284475](https://doi.org/10.5281/zenodo.13284475) (2024).
- [33] J. D. Torres Luna, K. Vilkelis and A. L. R. Manesco, *Probing valley phenomena with gate-defined valley splitters*, doi:[10.5281/zenodo.11091444](https://doi.org/10.5281/zenodo.11091444) (2024).
- [34] Y. Li, M. Amado, T. Hyart, G. P. Mazur and J. W. A. Robinson, *Topological valley currents via ballistic edge modes in graphene superlattices near the primary dirac point*, Communications Physics **3**(1) (2020), doi:[10.1038/s42005-020-00495-y](https://doi.org/10.1038/s42005-020-00495-y).
- [35] M. I. Katsnelson, K. S. Novoselov and A. K. Geim, *Chiral tunnelling and the klein paradox in graphene*, Nature Physics **2**(9), 620–625 (2006), doi:[10.1038/nphys384](https://doi.org/10.1038/nphys384).
- [36] M. I. Katsnelson, *Graphene: carbon in two dimensions*, Materials Today **10**(1), 20 (2007), doi:[https://doi.org/10.1016/S1369-7021\(06\)71788-6](https://doi.org/10.1016/S1369-7021(06)71788-6).
- [37] R. T. Weitz, M. T. Allen, B. E. Feldman, J. Martin and A. Yacoby, *Broken-symmetry states in doubly gated suspended bilayer graphene*, Science **330**(6005), 812–816 (2010), doi:[10.1126/science.1194988](https://doi.org/10.1126/science.1194988).
- [38] C. W. Groth, M. Wimmer, A. R. Akhmerov and X. Waintal, *Kwant: a software package for quantum transport*, New Journal of Physics **16**(6), 063065 (2014), doi:[10.1088/1367-2630/16/6/063065](https://doi.org/10.1088/1367-2630/16/6/063065).
- [39] J. W. McClure, *Band structure of graphite and de haas-van alphen effect*, Phys. Rev. **108**, 612 (1957), doi:[10.1103/PhysRev.108.612](https://doi.org/10.1103/PhysRev.108.612).
- [40] J. C. Slonczewski and P. R. Weiss, *Band structure of graphite*, Phys. Rev. **109**, 272 (1958), doi:[10.1103/PhysRev.109.272](https://doi.org/10.1103/PhysRev.109.272).
- [41] J. W. McClure, *Theory of diamagnetism of graphite*, Phys. Rev. **119**, 606 (1960), doi:[10.1103/PhysRev.119.606](https://doi.org/10.1103/PhysRev.119.606).
- [42] I. M. Flór, A. Lacerda-Santos, G. Fleury, P. Roulleau and X. Waintal, *Positioning of edge states in a quantum hall graphene pn junction*, Physical Review B **105**(24) (2022), doi:[10.1103/physrevb.105.1241409](https://doi.org/10.1103/physrevb.105.1241409).
- [43] J. Li, H.-B. Leng, H. Fu, K. Watanabe, T. Taniguchi, X. Liu, C.-X. Liu and J. Zhu, *Superconducting proximity effect in a transparent van der waals superconductor-metal junction*, Physical Review B **101**(19) (2020), doi:[10.1103/physrevb.101.195405](https://doi.org/10.1103/physrevb.101.195405).

A Model and simulation details

All the numerical simulations presented in this manuscript were obtained via a tight-binding implementation of Bernal-stacked bilayer graphene. The tight-binding model was implemented in Kwant [38], following the Slonczewski-Weiss-McClure parametrization [39–41] and using tight-binding parameters obtained via infrared spectroscopy [21]. We neglect the effects of spin-orbit coupling and therefore treat spins as a trivial degeneracy. Besides the pristine Slonczewski-Weiss-McClure tight-binding Hamiltonian $\mathcal{H}_{\text{pristine}}$, we add onsite modulations of the chemical potential μ and sublattice imbalance U to emulate the effects of multiple gate layers as

$$\mathcal{H}_{\text{onsite}} = \sum_n \psi_n^\dagger [U(\mathbf{r}_n)\text{sign}(\mathbf{r}_n \cdot \hat{z}) - \mu(\mathbf{r}_n)] \psi_n, \quad (1)$$

where $\psi_n = (c_n, c_n)^T$, c_n is an annihilation operator of an electron at the atomic site n .

Throughout the manuscript, we simulate mesoscopic devices with sizes $\sim 1\mu\text{m}$. To minimize the cost of the simulations, we rescale the tight-binding model by increasing the lattice constant as $\tilde{a} \mapsto sa$ and then adjusting the hopping parameters to preserve the low-energy Hamiltonian. We set $s = 10$ for most of the simulations, except for the data shown in Fig. 4 where we used $s = 20$.

The screening effects are included by smoothening the electrostatic potential. In our calculations, we set the potential at the interface between two regions with potentials V_1 and V_2 as

$$V(\mathbf{r}) = \frac{(V_1 - V_2)}{2} \left[1 + \tanh\left(\frac{|\mathbf{r} - \mathbf{r}_B|}{\chi}\right) \right] + V_2, \quad (2)$$

where χ is the screening length, and \mathbf{r}_B is the closest point at the boundary between the two regions. Typically $\chi \sim 25 - 50\text{nm}$ and we use $\chi = 25\text{nm}$ throughout the manuscript except if it is explicitly stated [42, 43]. Thus, the chemical potential is the average between the potential in the two layers

$$\mu(\mathbf{r}) = \frac{V_{\text{upper}}(\mathbf{r}) + V_{\text{lower}}(\mathbf{r})}{2}, \quad (3)$$

and the layer imbalance is the difference between the layer potentials

$$U(\mathbf{r}) = V_{\text{upper}}(\mathbf{r}) - V_{\text{lower}}(\mathbf{r}). \quad (4)$$

We fix $U(\mathbf{r}) = \pm 100\text{meV}$ far from the gate edges through the manuscript.

We compute the conductance across the devices via scattering formalism. All the calculations are performed at zero bias. For the two-terminal devices simulated in the manuscript, the zero-bias conductance is

$$G = \frac{2e^2}{h} \text{Tr}(tt^\dagger), \quad (5)$$

where t is the transmission matrix, and the factor of 2 comes from spin degeneracy.